Teaching Editorial

Image Fusion in Medicine: An Overview Using The CT-SPECT Model

With the widespread application of computer technology in medical imaging, digital images are now routinely produced in many different modalities. Specifically, detailed cross-sectional anatomic images are now obtained with either x-ray computed tomography (CT) or magnetic resonance imaging (MRI), while cross-sectional functional images are produced by single-photon emission tomography (SPECT) or positron emission tomography (PET). Subsequent comparison of these images usually is accomplished by visual analysis, with the observer mentally integrating the data prior to rendering an interpretation (*1,2*). Although this approach is adequate in most clinical situations, a more accurate comparison can be performed by directly combining the images with the aid of a computer in order to extract and manipulate the desired information. This latter technique, image fusion, has the additional advantages of (1) correcting for variability in orientation, position, and dimension; (2) allowing precise anatomic-physiologic correlation; and (3) permitting regional quantitation (*3*).

The purpose of this paper is to serve as an introduction to image fusion in medicine, using the CT-SPECT model. The topics covered include: (1) a brief description of the CT-SPECT model; (2) a discussion of the problems and assumptions of image matching; (3) a review of clinical approaches to matching; and (4) several potential applications. For a more in-depth explanation of pattern recognition and matching, including detailed mathematical descriptions of coordinate transformations and matching algorithms, the interested reader is referred to the physics, engineering, and computer graphics literature (*4–11*).

CT-SPECT MODEL

A detailed discussion of an image fusion system necessarily entails a thorough description of its individual components (*12*). For the SPECT-CT model, this would include: (1) the CT scanner, (2) the SPECT scanner; (3) the object to be imaged; (4) the relationship between the object and the scanners; (5) the viewing environment; and (6) the interpreter. Such a complete discussion is clearly beyond the scope of this paper, and may be found in the literature. The physical principles of x-ray CT and SPECT have been discussed thoroughly in several texts (*13,14*) and journal articles (*15–19*), while Brooks and Di Chiro (*20*) have described several common reconstruction algorithms. An excellent review article of the science of visual perception and image display terminals (*21*) recently has been published, and other authors have summarized the potential applications of automated image analysis (*22*) and artificial intelligence (*23*). The following discussion will, therefore, be limited to a few salient points regarding CT and SPECT resolution and lesion detection.

Three important, interrelated criteria of CT performance are uniformity, resolution, and precision. Uniformity refers to the accuracy of the equipment response in one area compared with another area. Nonuniformity may be due to beam hardening, detector flaws, poor geometry, and poor mathematical reconstruction (*13*). Resolution for high contrast objects is dependent upon pixel size, which is ~1 mm for a CT device with a whole-body scan circle of 50 cm and a 512 × 512 matrix. Typically the high contrast resolving power of a CT device should be 1.5 times that of the pixel width (*17*). Unfortunately, increasing the matrix size decreases the statistical precision of the data within each pixel, according to the relationship: $(\text{inaccuracy})^2 \sim (\text{resolution})^3$ (*16*). Although CT scanners are very sensitive and can detect attenuation differences as low as 0.5% (*15*), low contrast resolution or visibility is primarily dependent upon precision and object size (*13*). Decreased precision (quantum mottle or picture grain) can be improved by either decreasing the matrix size or increasing the patient radiation dosage according to the relationship: Picture grain $\sim 1/\sqrt{\text{dosage}}$ (*16*). Ultimately, whether a suspected lesion will be detected by CT scanning is dependent upon several factors including: the attenuation coefficient of the lesion compared to the background; the size and shape of the lesion; the homogeneity of the lesion and the background; and the presence of noise artifacts in the picture (*15*).

Similar performance criteria also are applicable to SPECT scanning with the additional constraint of poor counting statistics due to geometric and dosimetric considerations and detector inefficiency. A conventional gamma camera can detect only ~0.03% of photons emitted from a source in its field of view (*18*). Due to the inherent quantum mottle in SPECT, uniformity is critical and nonuniformities should be limited to the 1% level. Nonuniformity may be due to nonlinearities, regional variation to energy response, and sensitivity variations that may be corrected with appropriate linearity, energy, and sensitivity correction map tables (*18*). The limit-

For reprints contact: Lawrence C. Swayne, MD, Dept. of Diagnostic Radiology, Morristown Memorial Hospital, 100 Madison Ave. Morristown, NJ 07960.

ing factor in SPECT resolution and sensitivity is the collimator, which transforms an intrinsic resolution of 3.5 mm into a system resolution of 10 to 20 mm, depending on the distance from the collimator face (*18,19*). Once again, resolution may improve with a smaller pixel size, at a cost of decreased precision. The usual SPECT pixel size is 6 mm for a 15" large field of view gamma camera and a 64 × 64 matrix, and typical full width at half maximum values for a rotating gamma camera system vary from 14 to 17 mm, depending on the radius of rotation and choice of collimator. Compared to planar scintigraphy, SPECT has the additional advantages of three-dimensional localization and improved contrast resolution, despite a decreased spatial resolution. Jaszczak (*24*), using cold spheres in a uniform background, demonstrated an improved contrast ranging from 0.32 to 0.54, depending on the object size and location within the phantom. Improvements in scatter correction can be expected to further enhance accurate quantitation (*25*). Quantitation of small object volumes also is dependent upon the object size, and the SPECT system can be calibrated using small object phantoms (*26*). Thus, knowledge of the response of the imaging system is required to extract meaningful quantitative data and also is important for optimal filter selection (*27*). Finally, consideration of the sampling theorem (the minimum wavelength that can be observed when sampling data is spectrally analyzed is twice the spacing between the sampled points) limits the size of lesions that can be measured (*17*).

Differences in the response of the CT and SPECT scanners to the anatomical and functional features of the same stimulus may create additional problems when the images are fused. Intense activity may make a structure appear abnormally enlarged, while the situation may be reversed with low activity (*28*). Absence of function in an anatomically normal area may be interpreted as absence of the corresponding structure (*28*). Other sources of error that may affect both CT and SPECT are partial volume averaging and motion artifacts. Discrepancies between CT and PET or SPECT due to partial volume averaging may occur from: (1) differences in slice thickness between CT (10 mm) and SPECT (double thickness = 12 mm) (*29*); (2) slight axial differences in the central planes of comparable slices; and (3) differences in body positioning or gantry angulation. These problems may be partially alleviated by using rigid head holders with anatomic markers for brain studies (*30*), and by careful attention to reproducibly positioning the patient using external markers (*3*). Attention to patient comfort during the examination may minimize patient motion. An additional minor disadvantage of image fusion is the loss of resolution and contrast on the CT portion of the composite image, which results from the downward interpolation of the CT matrix size and the available gray scale in order to accommodate the SPECT image (*1,3*).

IMAGE MATCHING

Once the limitations of resolution and lesion detection are understood for the CT-SPECT model, image matching may be discussed. Since the studies are initially collected and processed by two different computers, preliminary data transfer to a common computer system is required. This can be accomplished through either cable or a common magnetic storage medium, providing that the appropriate software for data transmission and reception is available. Alternatively, data may be transferred using a digital camera and video acquisition board in the common computer system (*31*). While this latter method does not require additional data transmission and reception software, some resolution and contrast is invariably lost even before further data processing is undertaken. Finally, computer fusion may be bypassed entirely using direct film superimposition with registered transparencies (*32*); however, this simple approach does not permit further computer processing or quantitation.

Two basic assumptions of image matching are that: (1) the two images must be in the same representational form; and (2) there exists a similarity relationship between the two images (*12,33*). These assumptions are satisfied for the CT-SPECT model because (a) the images are both in cross-sectional form, and (b) a similarity relationship exists between images when corresponding slices at the same level in the body are compared. Images that fulfill these matching assumptions may still differ from each other by spatial distortions or image displacements (Fig. 1). Common image displacements include: expansion, inversion, rotation, horizontal translation, vertical translation, horizontal shearing, vertical shearing, and elastic deformation (*4,9,12*). For each image displacement there is a corresponding image transformation (scaling, reflection, rotation, horizontal translation, vertical translation, horizontal stretching, vertical stretching, and rubber disformation) that can map one Cartesian coordinate

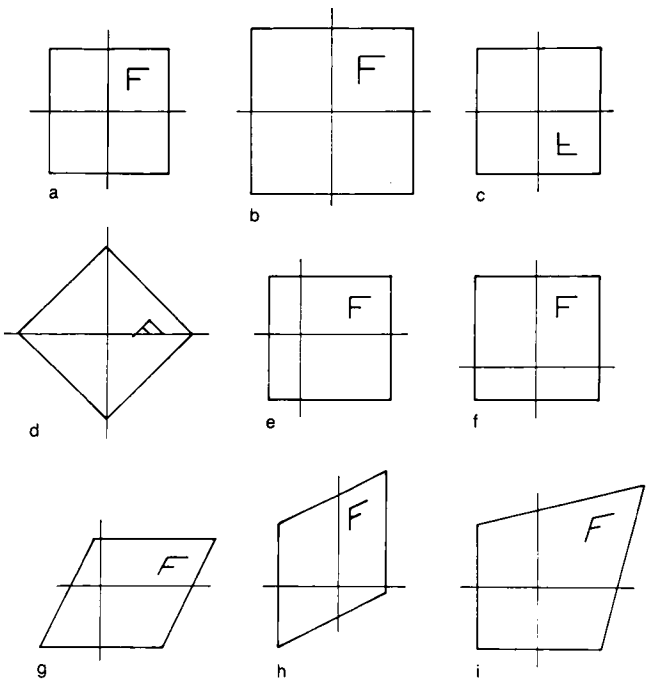

FIG. 1. Common image displacements superimposed on (a) Cartesian coordinate system, (b) expansion, (c) inversion, (d) rotation, (e) horizontal translation, (f) vertical translation, (g) horizontal shearing, (h) vertical shearing, and (i) elastic deformation.

system into another (*9,22*). Transformations are said to commute with each other if they produce the same result regardless of the order in which they are performed (e.g., rotation and scale changes commute) (*9*). Thus, CT and SPECT images can be matched (registered) with each other, if common landmarks points can be identified in each image.

Geometric transformations of image displacements will result in fractional pixel shifts which then must be assigned an appropriate gray scale level by interpolation. The simplest interpolation scheme is zero-order interpolation (nearest neighbor value); however, this often results in dramatic gray level changes between adjacent pixels, creating a "blocky" appearance. A more desirable approach, which preserves edges, is the application of bilinear interpolation using the values from the four nearest pixels. Advanced techniques such as bicubic spline interpolation and sinc or similar functions are computationally expensive and offer no significant additional advantages (*34*).

CLINICAL APPROACHES TO IMAGE MATCHING

An image fusion hierarchy of varying complexity (Table 1) can be conceptualized with the mathematically more sophisticated algorithms offering increased flexibility (*22*). Separate mental integration and computer quantitation of the images is adequate in most routine clinical situations (*1,2,35*). Direct image superimposition can be accomplished with film transparencies (*32*), following appropriate magnification correction. Unfortunately, this simple approach lacks the flexibility of computer-based matching algorithms, is not applicable in three dimensions, and also does not provide data quantitation. Plastic distortion (*22*) consists of rotating the image or changing the relative length of size along an axis. It is comprised of scaling, rotation, and translation transformations and has been used in both two- (*31,36,37*) and three-dimensions (*28, 38,39*) with rigid head holders to study brain function. A more accurate matching scheme can be achieved using the above transformations in conjunction with horizontal and vertical shearing transformations (*4*). This latter method has been successfully employed in chest and abdominal imaging (*3,40*). Automated image alignment (*4,41*) may obviate the need for inefficient and expensive operator interaction.

Rubber disformation is the most complex matching algorithm and is capable of both global and local registration (*12, 22,42*). Intuitively, this technique is analogous to deforming or stretching the data image on a rubber sheet in order to conform to the model image. Initially, the computer identifies certain pre-established primitive features or elements (e.g., straight-edge detectors, curved-edge detectors, circle detectors, and intersection detectors) (*10*) within both the data and model images. Following a global matching process, the primitive features of the data image are brought into fine local registration with the corresponding primitive features of the model image. This final local matching process may be governed by a cost analysis function in which optimal alignment occurs when the cost of deformation is comparable to the cost of similarity (*12*). Alternatively, the process may be monitored by computer-based optimization programs such as dynamic programming (*5,43*). Cross-correlation coefficients can be used to determine the maximum similarity between the images (*42*). If commonly identifiable points (often referred to as control points) can be located on both images, the registration can be evaluated based upon how well these points are matched (*10*).

TABLE 1. Image Fusion Hierarchy

1. Direct visual comparison
2. Image superimposition
3. Plastic distortion
   a. Scaling, rotation, translation (SRT) transformations
   b. SRT and shearing transformations
4. Rubber disformation

In addition to the basic matching algorithms described above, an ideal program would also contain; (1) menu driven commands for ease of operation; (2) simultaneous display of both images for direct comparison; (3) the opportunity to window individual images during each step of the program, in order to optimally visualize specific regions of interest (ROIs); and (4) the ability to quantitate the success of image registration. Since manual operator alignment may be subjective (*1*) and inefficient (*41*), an automated alignment routine could facilitate computer processing. Other desirable software features would include: (1) an edge finding algorithm (e.g., thresholding, derivative, or region growing techniques) to outline various regions of interest (*44*); and (2) the ability to provide quantitative data (*1,2,31,35–39,45–47*). The final composite image may be displayed in several different formats (blink mode alternating between the SPECT and CT images, simultaneous display using translucency, selected portions of the SPECT image in color superimposed on a gray-scale CT image, selected SPECT ROIs superimposed on a gray-scale CT image, and SPECT color isocontours superimposed on a gray-scale CT image), depending upon operator preference and the capability of the video display terminal (*21*).

POTENTIAL APPLICATIONS

The primary advantage of image fusion in medicine is precise anatomical-functional correlation (*3,28,30,38,42,47, 49*). Functional abnormalities detected with the inherently low resolution images of SPECT or PET can be precisely localized on the anatomic images of CT or MRI. The technique has been employed primarily for quantitative brain studies (*2,28,31,35–39,42,45–47*) with registration accuracies of < 2 mm (*31,39*). Some authors (*2,48,49*) have advocated the conversion of all images to a stereotactic atlas in order to provide a standardized frame of reference and to facilitate the planning for neurosurgical biopsies and operations as well as radiation therapy. Controversy exists, however, regarding which method (direct matching with CT or MRI versus matching through an intermediary standardized stereotactic atlas) produces the closest registration in three dimensions (*2, 45*).

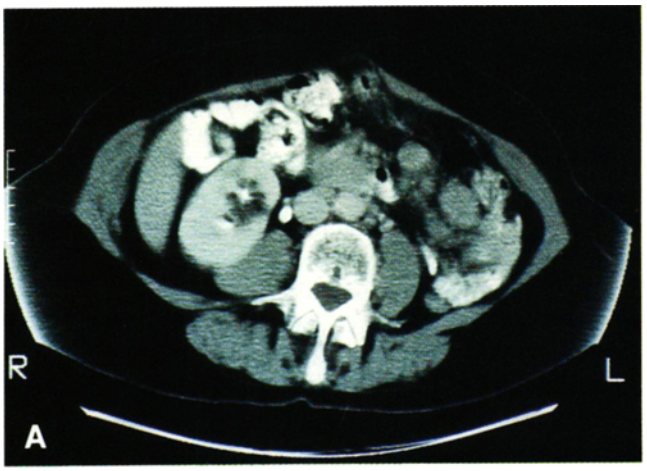

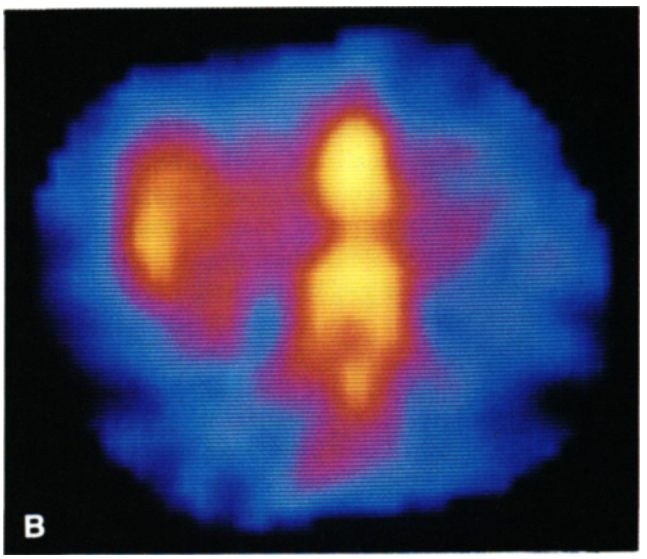

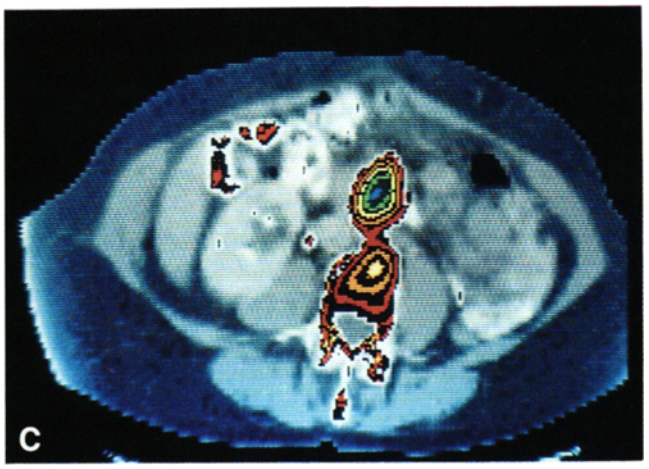

FIG. 2. CT scan of a 65-yr-old female with large cell nonHodgkins lymphoma demonstrates a "mass" at the level of the aortic bifurcation, consistent with either recurrent disease or an unopacified bowel loop. (B) The ^{67}Ga SPECT scan demonstrated increased activity in the lower abdomen, suggestive of adenopathy. (C) Composite SPECT-CT image. The composite study demonstrated a correspondence between the two abnormalities, compatible with recurrent lymphoma.

Image fusion also has been applied to chest and abdominal imaging (*1,3,40,50*). Matching of CT and SPECT images may be useful for body contouring and attenuation correction of SPECT images using the attenuation coefficients of the CT image (*14*). Unfortunately, less than perfect registration may cause many undesirable artifacts. Unique advantages of composite images in whole-body imaging include: (1) establishing the physiologic status of ambiguous CT objects (Fig. 2).; (2) identification of minimal anatomic abnormalities on CT which are of pathologic significance; and (3) planning for percutaneous biopsies or surgery in selected cases (*3*). Recently, image fusion also has been employed with SPECT monoclonal antibody imaging (*50*) for early lesion detection and localization and possible future quantitative analysis.

SUMMARY

Image fusion is a powerful tool in the investigation of structural-functional relationships. Optimal utilization is dependent upon a knowledge of both the limitations of a particular imaging system as well as an understanding of matching assumptions and algorithms. Unique advantages of this technique include: (1) accurate anatomical-functional correlation; (2) early identification and localization of selected pathologic lesions; and (3) quantitation of functional ROIs with poorly delineated boundaries. Further studies will be required in order to establish the precise role of image fusion in clinical and research settings.

Lawrence C. Swayne
Isaac L. Kaplan
Morristown Memorial Hospital
Morristown, NJ

ACKNOWLEDGMENTS:

The authors gratefully acknowledge the assistance of Mr. Simon Lam and Mr. Jessie Trivino for their constructive criticisms during the preparation of the manuscript.

REFERENCES

1. Pitcher EM, Stevens PH, Davies ER, et al. Transfer and combination of digital image data. *Br J Radiol* 1985;58:701–703.

2. Fox PT, Perlmutter JS, Raichle ME. A stereotactic method of anatomical localization for positron emission tomography. *J Comput Assist Tomogr* 1985;9:141–153.

3. Kaplan IL, Swayne LC. Composite SPECT-CT: Applications in chest and abdominal imaging (Abstract). *J Nucl Med* 1988;29:974.

4. Barber DC. Automatic alignment of radionuclide images. *Phys Med Biol* 1982;27:387–396.

5. Fischler MA, Elschlager RA. The representation and matching of pictorial structures. *IEEE Trans Comput* 1973;C-22:67–92.

6. Hueckel MH. An operator which locates edges in digitized pictures. *JACM* 1971;18:113–125.

7. Hueckel MH. A local visual operator which recognizes edges and lines. *JACM* 1973;20:634–647.

8. Rosenfeld A. Connectivity in digital pictures. *JACM* 1970;17:146–160.

9. Rosenfeld A, Kak AC. *Digital Picture Processing*, Vol. II, 2nd ed. New York: Academic Press; 1982:10–54.

10. Stockman G, Kopstein S, Benett S. Matching images to models for registration and object detection via clustering. *IEEE Trans Pattern Anal Machine Intell* 1982; PAMI-4:229–241.

11. Tobler WR. Comparing figures by regression. *Comput Graph* 1976; 12:193–195.

12. Bajcsy R. Three dimensional analysis and display of medical images. In: Reivich M, Alavi A, eds. *Positron Emission Tomography.* New York: Alan R. Liss; 1985:119–129.

13. Christiansen EE, Curry TS III, Dowdey JE. *An Introduction to the Physics of Diagnostic Radiology.* 2nd ed. Philadelphia: Lea & Febiger; 1978:329–360.

14. Croft BY. *Single Photon Emission Computed Tomography.* Chicago: Year Book Medical Publishers; 1986:1–306.

15. Bergstrom M, Sundman R. Picture processing in computed tomography. *AJR* 1976;127:17–21.

16. Hounsfield GN. Picture quality of computed tomography. *AJR* 1976; 127:3–9.

17. McCullough EC, Payne JT, Baker HL Jr, et al. Performance evaluation and quality assurance of computed tomography scanners with illustrations from the EMI, ACTA, and Delta scanners. *Radiology* 1976;120:173–188.

18. Heller SL, Goodwin PN. SPECT instrumentation: Performance, lesion detection, and recent innovations. *Semin Nucl Med* 1987;17:184–199.

19. Larsson SA. Gamma camera emission tomography. *Acta Radiol* 1980;363(suppl):1–75.

20. Brooks RA, DiChiro G. Theory of image reconstruction in computed tomography. *Radiology* 1975;117:561–572.

21. Kundel HL. Visual perception and image display terminals. *Radiol Clin North Am* 1986;24:69–78.

22. Ackerman L. Toward automated image analysis: Future possibilities in historical perspective. *Radiol Clin North Am* 1986;24:79–85.

23. Siegel JA, Levin K, Rada R, Ziskin MC. Expert systems: Applications of artificial intelligence in medicine. *J Nucl Med Technol* 1986;14:175–181.

24. Jaszczak RJ, Whitehead FR, Lim CB, Coleman RE. Lesion detection with single-photon emission computed tomography (SPECT) compared with conventional imaging. *J Nucl Med* 1982;23:97–102.

25. Jaszczak RJ, Greer KL, Floyd CE Jr, Harris CC, Coleman RE. Improved SPECT quantification using compensation for scattered photons. *J Nucl Med* 1984;25:893–900.

26. Kircos LT, Carey JE Jr, Keyes JW Jr. Quantitative Organ visualization using SPECT. *J Nucl Med* 1987;28:334–341.

27. Galt JR, Hise HL, Garcia EV, Nowak DJ. Filtering in frequency space. *J Nucl Med Technol* 1986;14:152–160.

28. Bohm C, Grietz T, Kingsley D, Berggren BM, Olsson L. Adjustable computerized stereotaxic brain atlas for transmission and emission tomography. *AJNR* 1983;4:731–733.

29. Mazziotta JC, Phelps ME, Plummer D, et al. Quantitation in positron emission computed tomography: 5. physical-anatomical effects. *J Comput Assist Tomogr* 1981;5:734–743.

30. Bergstrom M, Boethius J, Eriksson L, Grietz T, Ribbe T, Widen L. Head fixation device for reproducible position alignment in transmission CT and positron emission tomography. *J Comput Tomogr* 1981;5:136–141.

31. Miura S, Kanno I, Iida H, et al. Anatomical adjustments in brain positron emission tomography using CT images. *J Comput Assist Tomogr* 1988;12:363–367.

32. Higa T, Tanada S, Taki W, et al. Superimposition of krypton-81m single photon emission CT and x-ray CT images for cerebral blood flow evaluation. *J Comput Assist Tomogr* 1983;7:37–41.

33. Williams DL, Ritchie JL, Hamilton GW. Implementation of a digital image superposition algorithm for radionuclide images: An assessment of its accuracy and reproducibility. *J Nucl Med* 1978;19:316–319.

34. Barnes GT, Lauro K. Image processing: Basic concept and terminology. In: *Computers in Medical Physics.* Philadelphia: American Association of Physicists in Medicine, Summer School; 1988.

35. de Leon MJ, George AE, Ferris SH, et al. Regional correlation of PET and CT in senile dementia of the Alzheimer type. *AJNR* 1983;4:553–556.

36. Widen L, Blomqvist G, Greitz T, et al. PET studies of glucose metabolism in patients with schizophrenia. *AJNR* 1983;4:550–552.

37. Adair T, Karp P, Stein A, et al. Computer assisted analysis of tomographic images of the brain. *J Comput Assist Tomogr* 1981;5:929–932.

38. Martin WRW, Grochowski E, Palmer M, et al. Correlation of structural and functional images in the same patient (Abstract). *J Nucl Med* 1987;28:634.

39. Pelizzari CA, Chen GTY, Halpern H, et al. Three dimensional correlation of PET, CT, and MRI images (Abstract). *J Nucl Med* 1987;28:682.

40. Moskowitz GW, Vaugeois JC, Schiff RG, et al. Improvement of SPECT lung perfusion physiology with CT high resolution structural anatomy (Abstract). *J Nucl Med* 1986;27:1038.

41. Appledorn CR, Oppenheim BE, Wellman HN. An automated method for the alignment of image pairs. *J Nucl Med* 1980;21:165–167.

42. Bajcsy R, Lieberson R, Reivich M. A computerized system for the elastic matching of deformed radiographic images to idealized atlas images. *J Comput Assist Tomogr* 1983;7:618–625.

43. Beveridge GSG, Schechter RS. *Optimization: Theory and Practice.* New York: McGraw-Hill Book Co, 1970:679–702.

44. Keller JM, Edwards FM, Rundle R. Automatic outlining of regions on CT scans. *J Comput Assist Tomogr* 1981;5:240–245.

45. Mountz JM, Stafford-Schuck K, Koeppe R. Comparison of MRI and the stereotactic method for localization of brain structures on 0-15-H20 PET scans (Abstract). *J Nucl Med* 1987;28:702.

46. Evans AC, Beil C, Marrett S. MRI-PET correlation using an adjustable ROI atlas (Abstract). *J Nucl Med* 1987;28:1070.

47. Bergstrom M, Martin W, Li D, et al. Correlation of PET, CT and NMR images in the same patient. *Neurology* 1984;34(suppl 1):228.

48. Kelly PJ, Kall BA, Goerss S. transposition of volumetric information derived from computed tomography scanning into stereotactic space. *Surg Neurol* 1984;21:465–471.

49. Schad LR, Boesecke R, Schlegel W, et al. Three dimensional image correlation of CT, MR, and PET studies in radiotherapy treatment and planning of brain tumors. *J Comput Assist Tomogr* 1987;11:948–954.

50. Kramer EL, Noz ME, Sanger JJ, et al. CT/SPECT fusion for correlation of monoclonal antibody (MOAB) SPECT and abdominal CT. 35th Annual Meeting Annual Society of Nuclear Medicine (works-in-progress). San Francisco: 1988.